Co^{2+} Binding Cysteine and Selenocysteine: A DFT Study

Riccardo Spezia,* Guewen Tournois, Thierry Cartailler, Jeanine Tortajada, and Yannick Jeanvoine

Laboratoire Analyse et Modélisation pour la Biologie et l'Environnement, Université d'Evry Val d'Essonne, UMR 8587 CNRS, Bat Maupertuis, Bd F. Mitterrand, 91025 Evry, Cedex, France

Received: March 10, 2006; In Final Form: May 19, 2006

In this paper we report structural and energetic data for cysteine and selenocysteine in the gas phase and the effect of Co^{2+} complexation on their properties. Different conformers are analyzed at the DFT/B3LYP level of both bound and unbound species. Geometries, vibrational frequencies, and natural population analysis are reported and used to understand the activity of these species. In particular, we have focused our attention on the role of sulfur and selenium in the metal binding process and on the resulting deprotonation of the thiol and seleniol functions. From the present calculations we are able to explain, both from electronic structure and thermochemical point of views, a metal-induced thiol deprotonation as observed in gas-phase experiments. A similar process is expected in the case of selenocysteine. In fact, cobalt was found to have a preferential affinity with respect to thiolate and selenolate functions. This can be related to the observation that only S and Se are able—in thiolate and selenolate states—to make a partial charge transfer to the cobalt thus forming very stable complexes. Globally, very similar results are found when substituing S with Se, and a very small difference in cobalt binding affinity is found, thus justifying the use of this substitution in X-ray absorption experiments done on biomolecules containing cysteine metal binding pockets.

1. Introduction

Understanding interactions between transition metals and amino acids is a key feature in the comprehension of many biochemical and biophysical problems, from natural occurring metalloprotein chelation to human and environmental toxicology.[1] With such an importance, it has become the subject of several theoretical and experimental studies in the past few years.[2−6] It is now well recognized that the binding of metal ions to biomolecules is fundamental for their biochemical activities. From a chemical point of view, metal binding can have a structuring effect on the biomolecule—in other words it can lead to a specific three-dimensional structure in the biomolecule. Furthermore, metal binding can also induce chemical reactions such as deprotonation of specific sites of the biomolecule.[7] Deprotonation of chemical functions in biomolecules appears as a common effect of metal binding, and in some cases it can even be directly related to the biological activity of the molecule.[8−11] Deprotonation of peptides and proteins induced by metal cations can occur both in their main chain and in their side chain.[7,12] The most relevant amino acids able to bind metal cations are the side chains of histidine, cysteine, aspartic acid, and glutamic acid. Cysteine is the only naturally occurring thiol-containing amino acid, giving its unique and fundamental properties in structure and activity of biomolecules. In particular, it is recognized that coordination of metal cations can be achieved through sulfur sites in a variety of proteins and metalloenzymes.[13−16] X-ray structures available in the Protein Data Bank (PDB) are consistent with deprotonated cysteines, so that metal binding occurs via thiolate groups.[17] At physiological pH, one should note that cysteine side chains with typical pK_a values between 8 and 9 would be protonated in metal-free proteins.[18−20] Binding to a metal cation causes the cysteine's pK_a to drop,[21] thus facilitating a thiol to thiolate chemical reaction under physiological conditions. The change in cysteine protonation state at neutral pH is therefore a typical example of a metal-assisted process.

Selenium is a chalcogen element located just below sulfur on the periodic table, and thus there are not only close similarities but also striking differences between these two elements in terms of their chemistry and biochemistry.[22] Selenium can replace sulfur in cysteine and methionine, thus forming selenocysteine and selenomethionine. Proteins containing selenium play a variety of important roles in cellular activity.[23,24] For example, a biological function of selenoprotein P (i.e. its important role in delivering hepatic selenium to specific tissues) was recently confirmed.[25,26] While the functions of selenoprotein P are not certain, one role may concern chelation of heavy metals.[23] In some cases selenium seems to have an important role in protection against metal toxicity.[27,28] These findings could suggest a specificity of Se in binding metals. On the other hand, selenium substitution is a powerful ligand-directed technique for determining metalloprotein coordination structures using X-ray absorption spectroscopy (XAS).[29,30] This implies, in apparent contrast with the biological specificity reported, a strong similarity between S and Se concerning metal interaction, as pointed out by Peariso et al. from XAS of zinc binding to cysteine and selenocysteine in methionine synthase.[29]

Our present contribution is a first attempt to investigate from a theoretical point of view the interaction of Co^{2+} with cysteine and selenocysteine. This metal, needed at trace level in organisms for the biosynthesis of vitamin B12, is also a typical polluting agent issue from several industrial processes. It is also an important radioactive contaminating species, especially the ^{60}Co isotope. It can be complexed by biological systems containing cysteine, as other transition metals. We are especially

* To whom correspondence should be addressed. Tel: +33-1-69 47 76 53. Fax: +33-1-69 47 76 55. E-mail: rspezia@univ-evry.fr.

10.1021/jp0614998 CCC: $33.50
Published on Web 07/15/2006

interested in understanding the physical basis of such a complexation. At this end, our group has begun a systematic study of different biomolecules containing cobalt in the gas phase combining different theoretical and experimental approaches.[31−33] In the present contribution we use density functional theory (DFT) to identify the structures of different Co^{2+} complexes with cysteine and selenocysteine and the gas-phase thermochemistry to study metal binding and metal induced cysteine and selenocysteine deprotonation.

The outline of the remainder of the text is as follows. In section 2.1 we describe the methods employed to solve electronic structure problems. In section 2.2 we describe the reactions considered for thermochemical analysis. Then we first show results obtained with the present computational setup on free cysteine and selenocysteine (section 3), and then we present results obtained when Co(II) binds amino acids (section 4). In section 5 we summarize and conclude.

2. Computational Methods

2.1. Structure Determination. Molecular geometries of the considered structures were optimized using DFT with the hybrid B3LYP functional.[34] Previous theoretical calculations have shown that the B3LYP is a reliable functional to study transition-metal−ligand systems,[35−37] and it was recently pointed out also its reliability to describe the interaction between cobalt and glycine[38] or glycylglycine.[39] Geometry optimizations and frequency calculations on the optimized structures have been performed using the following basis set: for Co the (14s9p5d) primitive set of Wachters[40] supplemented with one s, two p, and one d diffuse functions[41] and one f polarization function[42] and 6-31++G(d,p) for C, N, O, S, Se, and H—hereafter noted as basis set I. This basis set is a good compromise between computational costs and results reliability, as recently pointed out by Constantino et al. when studying cobalt binding glycylglycine.[39] To better understand the role of atomic basis sets, taking the geometries obtained with basis set I, we have performed single point energy calculations with a larger basis set corresponding to the following: Co basis is based on the (14s9p5d) primitive set of Wachters[40] supplemented with one s diffuse function, two p diffuse functions, and one d diffuse function[41] and two f polarization functions,[42] such that the final contracted basis set is [10s7p4d2f], while for N, C, O, S, Se, and H we used the 6-311++G(2df,2p) basis—hereafter noted as basis II. This is the same basis set recently used to investigate Co-glycine interactions by one of us.[38] Hereafter in the paper we will use the following notation: B3LYP/basisI for calculations with basis set I and B3LYP/basisII for calculations with basis set II (where the latter are single point calculations performed on B3LYP/basisI optimized geometries).

Net atomic charges have been obtained using the natural population analysis of Weinhold and co-workers.[43,44] We have considered in all the reported calculations Co(II) being in a quartet spin state, corresponding to the most stable state of hydrated cobalt in water[45,46] and also reported in the literature.[38] Moreover, all calculations done on our systems in the doublet spin state provide higher energy structures. Here, since the purpose of this work is not devoted to point out a possible role of different spin states, we will consider only the quartet spin state. Open shell calculations have been performed using an unrestricted formalism. All the above calculations have been performed with the Gaussian98 package.[47]

2.2. Thermochemistry. Cysteine (Cys) and selenocysteine (SeCys) gas-phase reactivity was investigated by standard thermochemical analysis performed on minimum energy structures in the harmonic approximation using standard expressions for an ideal gas in the canonical ensemble.[48] We have considered different reactions. First, we took into account protonation reactions of neutral amino acid (AH), i.e.

$$AH + H^+ \rightleftharpoons AH_2^+ \quad (1)$$

from which protonation affinity (PA) and gas-phase basicity (GPB) are defined as the opposite of enthalpy and free energy change, respectively (i.e. $PA = -\Delta H^0_{298}$ and $GPB = -\Delta G^0_{298}$).

Gibbs energy change is calculated as $\Delta G = \Delta H - T\Delta S$ where the entropy contribution is obtained by $T\Delta S = T[S(AH_2^+) - S(AH) - S(H^+)]$ with $T = 298.15$ K.

Further, the deprotonation reaction

$$AH \rightleftharpoons A^- + H^+ \quad (2)$$

is considered, for which we calculated ΔH^0_{298} and ΔG^0_{298} in the same way. We also took into account the deprotonation reaction of the Co^{2+} complexed species, $[CoCys]^{2+}$ and $[CoSeCys]^{2+}$, namely

$$[CoAH]^{2+} \rightleftharpoons [CoA]^+ + H^+ \quad (3)$$

Finally, the metal affinities (MAs) of Co^{2+} with Cys and SeCys, both in neutral and deprotonated forms, are calculated, analogously to PAs, i.e., $MA = -\Delta H^0_{298}$ of the cationization reaction

$$Co^{2+} + L \rightleftharpoons (CoL)^l \quad (4)$$

where L = AH, A^- with $l = 2+$ and $1+$, respectively. Basis set superposition error (BSSE) was estimated using the counterpoise method of Boys and Bernardi.[49] This effect was found to be of about 2 kcal/mol, similarly to what was found by Belcastro et al.[50] and Hoyau et al.[51] in similar systems.

3. Free Species

3.1. Structural Data. Optimized structures of neutral and protonated cysteine (Cys) and selenocysteine (SeCys) are shown in Figures 1 and 2, respectively, where we provide also some selected intramolecular distances. Relative energies of the different conformers obtained are reported in Table 1. For both neutral and protonated cysteine, results, in terms of geometries and relative energies, are in quite perfect agreement with literature DFT data performed with the same functional (B3LYP) and a different basis set (D95++(d,p)).[52] Selenocysteine structures, both neutral and protonated, are similar to the corresponding cysteine ones, while the energy order of neutral conformers presents some differences. Structure 1 is the most stable one for cysteine and selenocysteine. Apart from this structure, the energy order is different between selenocysteine and cysteine. Differences between cysteine and selenocysteine relative energies are relatively small, since they lie between 0.47 kcal/mol (structure 7) and 1.46 kcal/mol (structure 2). We may note that in some structures (2, 3, and 5) S to Se substitution modifies hydrogen bonds concerning thiol (seleniol) hydrogen atoms thus destabilizing these structures in selenocysteine with respect to the respective ones in cysteine. For protonated structures, results are almost identical between cysteine and selenocysteine. The energy order is exactly the same, and relative energies with respect to the minimum energy structure are very similar, the largest difference being ∼1 kcal/mol.

3.2. Thermochemical Analysis. Proton affinity and gas-phase basicity are calculated for cysteine and selenocysteine as

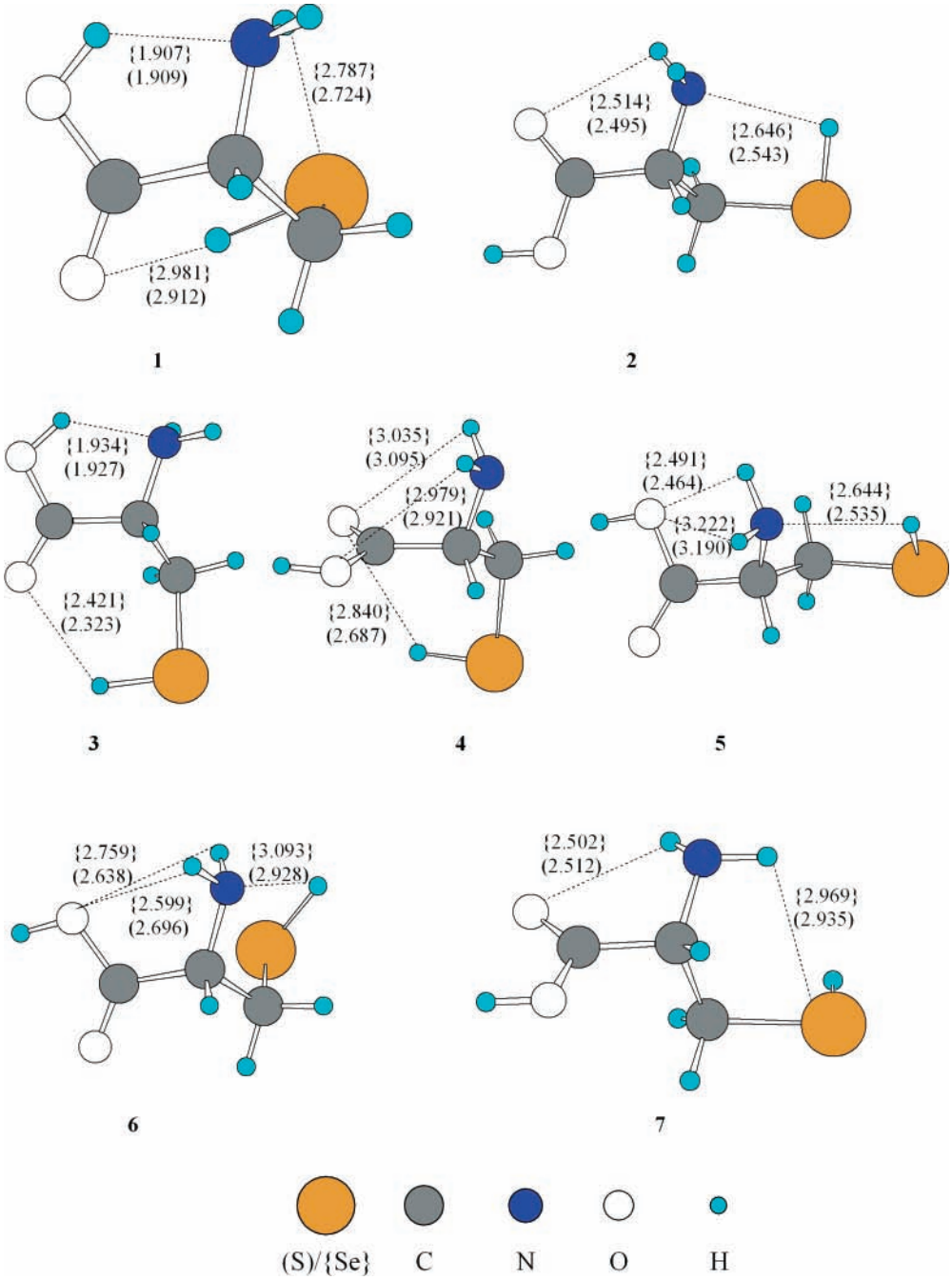

Figure 1. Structures of free Cys and SeCys, in neutral form. Some selected distances (in Å) are shown.

described in section 2.2 and reported in Table 2. Here we report also data for serine (Ser) taken from the literature (experimental[53,54] and theoretical[52]) and calculated in this study using the same procedure adopted for Cys and SeCys. For serine and cysteine our DFT calculations provide values almost identical to previous reported calculations[52] and very close to experiments.[53] Serine differs from cysteine only by the side-chain terminal group, the former bearing a hydroxyl group, the latter a thiol function. This substitution corresponds to an interchanging between two atoms belonging to the same group, VIa, in the periodic table. PA and GPB, both calculated and experimental, become smaller by changing from O to S. When substituting the thiol function with a seleniol function (SeH), this corresponds to a further step down the group VIa, but, quite surprisingly, both PA and GPB go up, as shown in Table 2. This nonmonotonic behavior was also found in thermochemical analysis of the deprotonation reaction as shown in Table 3. The deprotonation thermodynamics investigated (ΔH^0_{298} and ΔG^0_{298}) corresponds to the deprotonation of the hydroxyl function in serine and SH (SeH) function in cysteine (selenocysteine). SH and SeH functions were found, from our calculations in the gas phase, as the most acid groups in cysteine and selenocysteine, respectively.

4. Co(II) Complexes

4.1. Structural Data. First, we have determined the structures of complexes between Co(II) and deprotonated cysteine, i.e., $[Co(Cys\text{-}H)]^+$, and selenocysteine, i.e., $[Co(SeCys\text{-}H)]^+$. The $[Co(Cys\text{-}H)]^+$ species seems to be one of the most abundant in electrospray ionization mass spectrometry (ESI-MS) experiments done in our laboratory by Buchmann and co-workers.[31] All

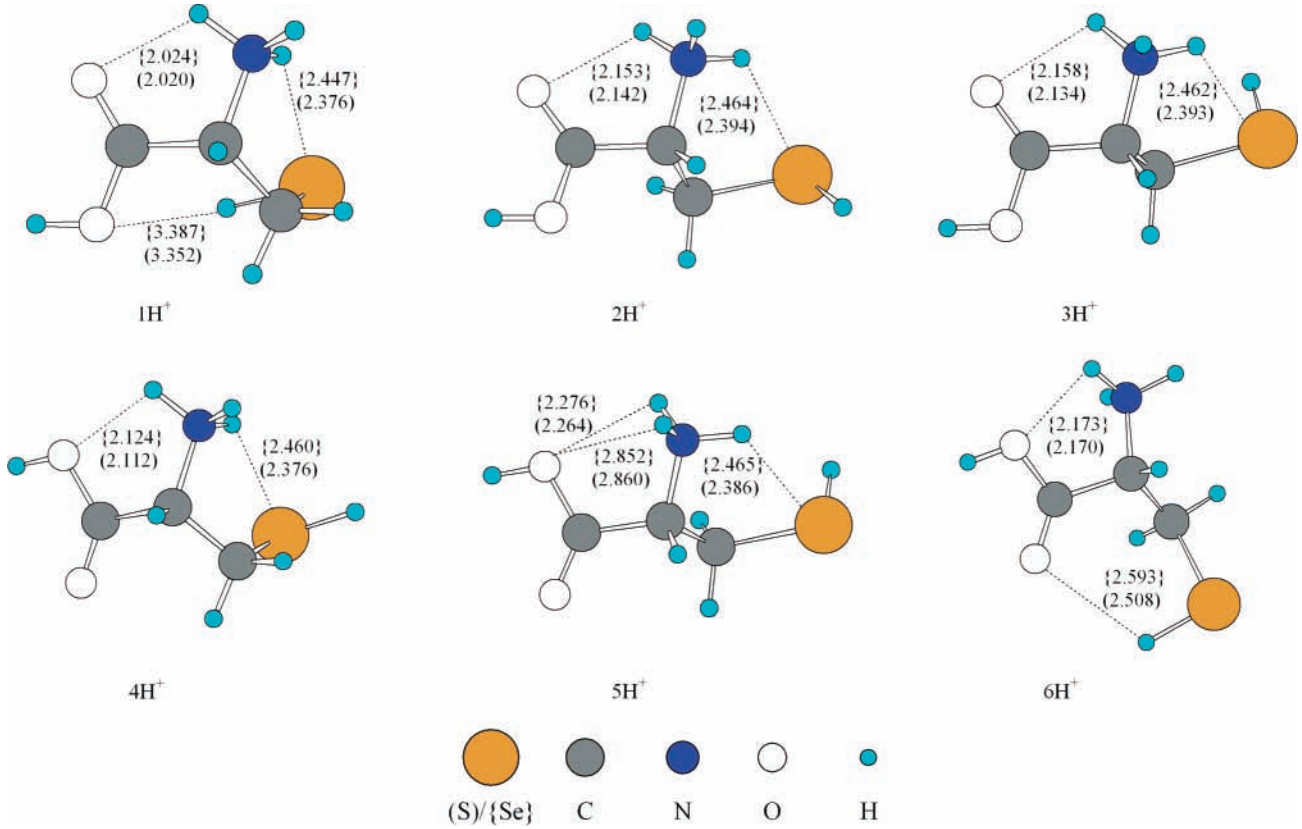

Figure 2. Structures of free Cys and SeCys, in protonated form. Some selected distances (in Å) are shown.

TABLE 1: Relative Energies (in kcal/mol) of Cysteine and Selenocysteine Configurations Studied in Neutral and Protonated Form[a]

	B3LYP/D95++(d,p)[b] cysteine neutral/ protonated	B3LYP/6-31++G** cysteine neutral/ protonated	B3LYP/6-31++G** Se-cysteine neutral/ protonated
1	0.00/0.00	0.00/0.00	0.00/0.00
2	1.44/0.09	1.26/0.20	2.72/0.52
3	2.52/1.19	2.36/1.33	3.61/1.25
4	2.59/4.90	2.47/4.97	2.97/3.57
5	2.81/5.02	2.62/5.07	3.93/4.86
6	3.00/9.97	2.90/9.72	2.16/10.66
7	3.31/−	3.36/−	3.83/−

[a] The same numeration of structures in Figures 1 and 2 is employed. [b] DFT results from ref 52.

TABLE 2: Proton Affinity and Gas-Phase Basicity (in kcal/mol) of Free Amino Acids Calculated at the B3LYP/6-31++G(d,p) Level

	PA			GPB		
	B3LYP	lit.[a]	exptl[b]	B3LYP	lit.[a]	exptl[b]
serine	218.3	218.3	218.6	210.5	210.6	210.5
cysteine	215.9	216.1	215.9	208.3	208.5	207.8
Se-cysteine	217.1			209.6		

[a] B3LYP/D95++(d,p) data from ref 52. [b] Experimental data from ref 53.

geometries of the considered $[Co(Cys-H)]^+$ ($[Co(SeCys-H)]^+$) structures are shown in Figure 3, and corresponding relative energies are collected in Table 4. As described in section 2.1, geometries are optimized at the B3LYP/basisI level of theory, and then, on these optimized structures, single point energy calculations are subsequently performed with the larger basis set (B3LYP/basisII) to investigate possible basis set effects. ZPE corrections are considered only at the B3LYP/basisI level and are also reported in Table 4.

TABLE 3: Thermochemical Data (ΔH^0_{298} and ΔG^0_{298} in kcal/mol) for the Gas-Phase Deprotonation Reaction of Neutral Serine, Cysteine, and Selenocysteine Obtained at the B3LYP/6-31++G(d,p) Level[a]

	ΔH^0_{298}		ΔG^0_{298}		ΔS^0_{298}[c]
	B3LYP	exptl[b]	B3LYP	exptl[b]	B3LYP
serine	330.1	332.7 ± 3.1	322.9	325.8 ± 3.0	24.0
cysteine	331.0	332.9 ± 3.1	323.9	326.0 ± 3.0	23.8
Se-cysteine	326.8		319.4		24.8
Co-Cys	107.8		100.4		24.9
Co-SeCys	108.9		101.4		25.3

[a] For Cys and SeCys the same quantities for the Co(II) complexed species are reported. For these calculations we used the most stable structures for each protonation state, i.e., structure 1S (with Cys and SeCys) of Figure 3 and structure I (with Cys and SeCys) of Figure 4. [b] Experimental data from ref 54. [c] Calculated ΔS^0_{298} in cal/(mol·K) are also shown.

$[Co(Cys-H)]^+$ and $[Co(SeCys-H)]^+$ potential energy surfaces become complicated by the presence of three possible deprotonation sites, SH (SeH), NH_2, and OH, and different cysteine (selenocysteine) spatial arrangements around Co^{2+}. Note that here and hereafter we use the following notation for ligands: S^- and SH for sulfur in thiolate and thiol function, respectively (Se^- and SeH for SeCys), O for carbonyl oxygen (C═O), O^- for carboxylate oxygen, OH for hydroxyl function, NH_2 for amine function, and NH^- for a deprotonated NH_2 group. We found seven stable structures where the SH (SeH) function is deprotonated (labeled 1S to 7S), three structures where the NH_2 function is deprotonated (labeled 1N, 2N, and 3N), and two structures where the OH site is deprotonated (1O and 2O). These structures are local minima both for Cys and SeCys. Moreover, the 1S structure was found to be the most stable one both for Cys and SeCys, and the energy order of the first four more stable structures is identical in all calculations. All these structures of

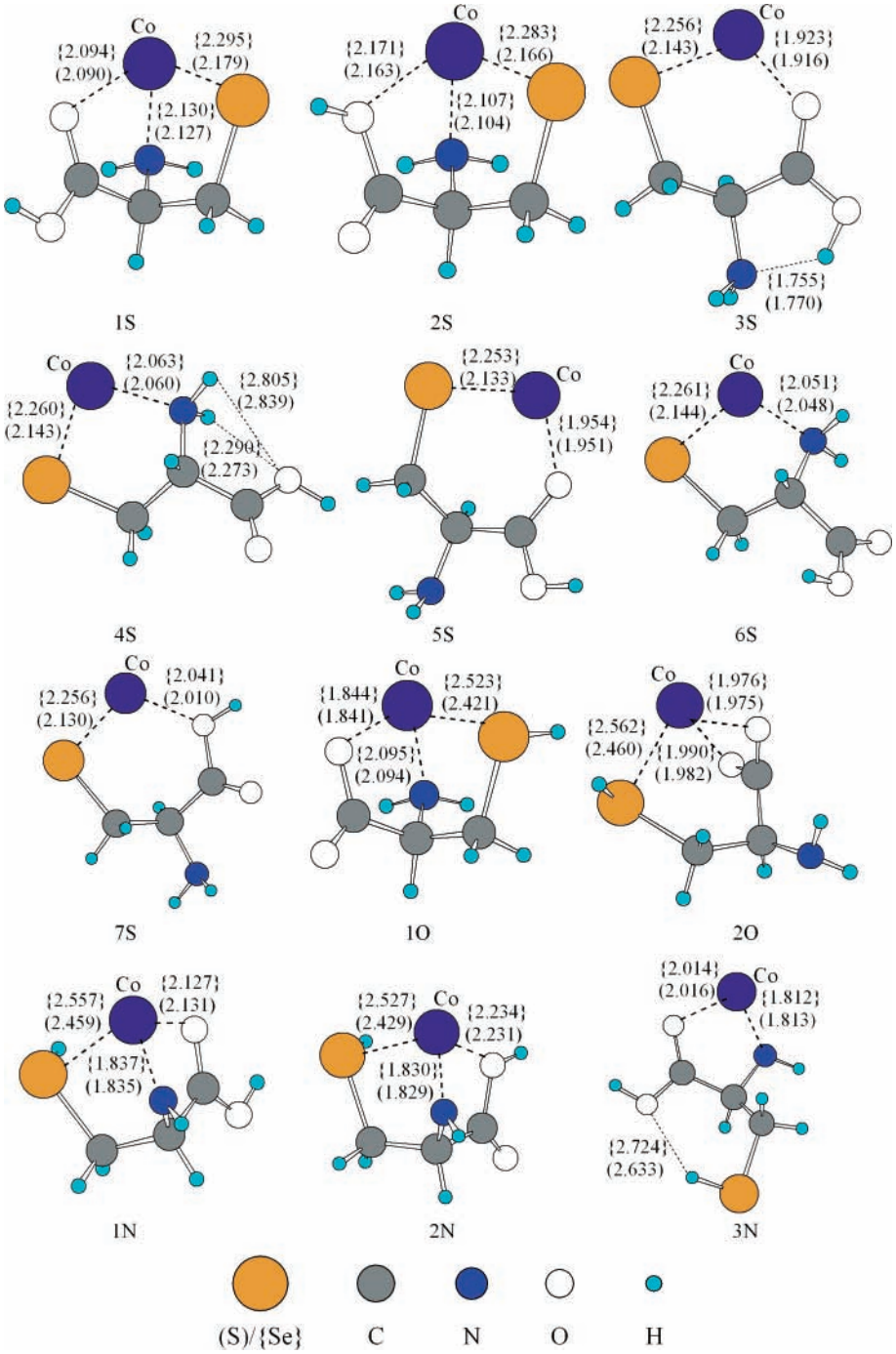

Figure 3. Structures of $[Co(Cys\text{-}H)]^+$ and $[Co(SeCys\text{-}H)]^+$ complexes obtained from B3LYP/basisI geometry optimization. Some selected distances (in Å) are shown. Thick dashed lines correspond to bond critical points as suggested by AIM analysis.

least energy (below ~17 kcal/mol) correspond to deprotonation of SH (SeH) and binding of Co^{2+} with S^- (Se^-).

The two most stable structures are tridentate complexes, while structures 3S and 4S—the third and fourth most stable ones, respectively—are bidentate, being Co^{2+} coordinated to S^- (Se^-) and carbonyl O or amine N, respectively. As we will describe further in details, calculations with the larger basis set (basisII in our notation) provide the same results, this strengthening the view of a tight and preferential binding of Co^{2+} to S^- (Se^-) function. Deprotonation of OH function provides a stable structure (1O) lying ~20 kcal/mol higher than 1S. In the selenocysteine case, this 1O-SeCys structure is slightly higher in energy than 1O-Cys, but we should note that the difference is very small (~1 kcal/mol). The other structure (2O) lies higher in energy of about 40 kcal/mol. This value decreases of about 3 kcal/mol by the inclusion of ZPE. This relative stabilization due to the ZPE correction is quite expected, since 2O is a particular tridentate structure where the NH_2 group is not bound to Co and thus this structure is intrinsically more flexible than other tridentate ones (like 1S). Deprotonation of NH_2 function provides three stable structures. The most stable one (1N) is also a tridentate structure being lower in energy for Cys (+21.07 kcal/mol relative to 1S) than for SeCys (+22.60 kcal/mol relative to 1S−SeCys), with a difference between Cys and SeCys of an amount similar to 1O case. We should note that tridentate conformations obtained with deprotonation of OH and NH_2 functions are energetically less stable than some bidentate conformations obtained with deprotonated SH (SeH) functions.

TABLE 4: Relative Energies (in kcal/mol) of $[Co(Cys-H)]^+$ and $[Co(SeCys-H)]^+$ Obtained at the B3LYP/basisI Level from SCF Energy (ΔE^{SCF}) and Adding ZPE Correction (ΔE^{+ZPE}) on Structures Reported in Figure 3[a]

	$[Co(Cys-H)]^+$		$[Co(SeCys-H)]^+$	
	ΔE^{SCF}	ΔE^{+ZPE}	ΔE^{SCF}	ΔE^{+ZPE}
1S	0.00(0.00)	0.00	0.00(0.00)	0.00
2S	+10.54(+10.79)	+10.08	+10.30(+10.60)	+9.85
3S	+14.84(+12.20)	+13.91	+12.41(+11.92)	+11.51
4S	+17.04(+17.06)	+16.62	+16.60(+16.56)	+16.18
5S	+21.71(+18.95)	+20.55	+21.41(+18.71)	+20.17
6S	+22.85(+21.81)	+22.25	+22.53(+21.34)	+21.90
7S	+35.88(+36.26)	+33.74	+36.45(+34.35)	+34.66
1N	+24.29(+23.14)	+21.07	+26.37(+26.35)	+22.60
2N	+33.98(+33.05)	+30.26	+36.14(+36.36)	+31.86
3N	+38.65(+37.69)	+35.02	+43.23(+42.14)	+39.12
1O	+20.55(+19.49)	+18.37	+21.89(+22.17)	+19.35
2O	+40.78(+39.01)	+37.57	+40.71(+47.27)	+37.16

[a] In parentheses we show data from B3LYP/basisII single point calculations done on the same geometries.

These important results show the affinity of Co(II) toward S^- and Se^- that will be investigated in more detail in the following.

We pause here to point out the effect of the basis set on these results. As previously mentioned, the basic picture is retained by using B3LYP/basisII calculations. Differences in relative energies are small for almost all structures. In some cases a difference of ~2 kcal/mol is observed, while the largest discrepancy (~6.5 kcal/mol) is found for the high-energy 2O structure. Energy order is almost identical, with some exceptions. In particular, the order between 1O and 5S (for Cys) or 6S (for SeCys) is inverted passing from B3LYP/basisI to B3LYP/basisII representation, due to the stabilization of 5S and 6S structures, respectively, with increasing the basis set. This can be due to a better Co−S(Se) interaction description when more diffuse functions are considered in the Co basis set and/or when a triple instead of a double-ζ basis set is used for S and Se, in conjunction with more diffuse functions. Other order inversions concern higher energy structures where, generally, few differences in relative energy are found. Note that B3LYP/basisII calculations are performed on B3LYP/basisI optimized structures (i.e. they are not necessarily minimum energy structures within the method) such that results should be used only to provide a global agreement between the two basis sets used.

In a further step, three prototypical structures of $[Co(Cys-H)]^+$ and $[Co(SeCys-H)]^+$ (1S, 1O, and 1N) among the 12 obtained were selected for a deeper investigation. These three conformations are the most stable ones for each deprotonation site, and hence they can help in clarifying the description of Co(II) interactions with the different possible ligands: S^- (Se^-), SH (SeH), O, O^-, NH_2, and NH^-. At this end, natural population analysis (NPA) of the complexes are performed. To understand the effect of Co^{2+} on the deprotonated Cys (SeCys) charge distribution, we have performed NPA calculations also on these three structures (1S, 1O, and 1N) without Co(II) cation, thus obtaining three $(Cys-H)^-$ (and three $(SeCys-H)^-$) structures (labeled 1S-Co, 1O-Co, and 1N-Co). Results are summarized in Table 5 where only charge distributions on Co, S (Se), N, and O atoms are shown. This choice is driven by the fact that we are interested in charge distributions of atoms that can act as electron donors toward the central metal atom (Co). We first should note that charge distributions are basically identical in case of Cys and SeCys, with few exceptions. The metal cation, formally charged +2 in the given oxidation state II, acts as an electrophilic species, since its charge decreases to [+1.15,+1.32] ([+1.10,+1.29] in the case of SeCys). Almost one unity of charge is transferred from Cys (SeCys) to the metal. In the 1S structure, where also the lower charge, +1.15 (+1.10), was found on cobalt, the S (Se) atom is mainly responsible for this charge transfer. In fact, in the free species the S (Se) atom possesses a negative charge fraction of −0.66 (−0.65). When a cobalt atom is bound, the charge on S (Se) drops to −0.19 (−0.10). This corresponds to a partial charge transfer, of about half a negative charge, from S (Se) to Co. This can explain the relatively large difference in stability (~20 kcal/mol) between S (Se) deprotonated structures and the others. Furthermore, in the structures where S (Se) is protonated (structures 1N and 1O) the charge on S (Se) is quite identical between free and bound species. Interestingly, the same phenomenon (i.e. no large differences in charge distribution between free and bound species) was found for the other atoms close to Co. In other words, in the case of structures 1N and 1O we cannot find a specific atom that acts as a nucleophilic species toward Co, albeit deprotonated N and O are present in those structures. A more detailed analysis of bonding properties was also carried out both using natural bond order[43,44] (NBO) and atom in molecule (AIM) methods.[55,56] Here we just summarize these bonding properties on the same prototypical structures (1S, 1O, and 1N) considered previously. Note that in Figures 3 and 4 thick dashed lines correspond to bond critical points found by AIM analysis performed on all the reported structures. In the 1S structure, NBO analysis reports a bond only between Co and S(Se), with a partial covalent character (70% on p orbitals of S(Se) and 30% on d orbitals of Co), while in the 1O structure the same analysis provides Co−O^- and Co−SH interactions with a mainly ionic character (85−90% on S(Se)/O atoms and 10−15% on Co). Similarly, in the 1N structure NBO analysis has pointed out mainly ionic interactions between Co and O and NH (85−95% on S(Se)/O/N and 5−15% on Co). In addition to that, in 1N also a weak covalent interaction between N p orbitals and Co d orbitals was found in NBO analysis. AIM analysis has also found these bonds being critical points, in agreement with NBO results. In particular, AIM analysis identifies the Co−S bond in the 1S structure as the partial covalent bond of Co with the largest density, that corresponds to the strongest covalent bond between Co and a ligand atom. On the other hand, in both 1O and 1N structures, Co−O and Co−N were reported to be the main ionic bonds with the largest density.

The characterization of these prototypical structures is completed by frequency analysis. In Table 6 we report frequencies and relative IR intensities of four selected modes over the 36 modes obtained by Hessian diagonalization done on these three structures (1S, 1O, and 1N with Cys and SeCys) after subtracting the first six translational and rotational modes of the complexes. These modes correspond to the Co−S(Se) stretching ($\nu_{Co-S(Se)}$) and to the three most intense modes: hydrogen bending (δ_H) where H atoms on N, O, and C contribute, C=O stretching ($\nu_{C=O}$), and OH stretching (ν_{OH}). The complete IR spectrum, with frequencies and relative intensities, is reported in the Supporting Information. We should note that IR experiments in the gas phase of such species are not present in the literature, to our knowledge. Hence the present study can be useful in order to give a preliminary guideline. The band assignment was done from the visualization of the obtained normal modes. Of course, we assign a mode to a particular chemical bond even if we are working with global normal modes. However, as typically happens for stretching modes, the stretching modes considered ($\nu_{Co-S(Se)}$, $\nu_{C=O}$, ν_{OH}) are well localized on the given chemical bond. Qualitatively,

TABLE 5: Charge Distributions on Cobalt and Polar Atoms Obtained from B3LYP/basisI NPA Calculations in the Minimized Geometry of the $[Co(Cys-H)]^+$/$[Co(SeCys-H)]^+$ Complexes, Values on the Left and Right of Columns, Respectively[a]

	1S	1S−Co	1O	1O−Co	1N	1N−Co
Co	+1.15/+1.10		+1.32/+1.29		+1.19/+1.19	
S/Se	−0.19/−0.10	−0.66/−0.65	+0.02/−0.16	−0.04/+0.05	+0.01/+0.14	−0.06/+0.02
N	−0.95/−0.96	−0.87/−0.88	−0.97/−0.97	−0.89/−0.89	−0.94/−0.96	−1.09/−1.09
O_v[b]	−0.69/−0.69	−0.61/−0.61	−0.80/−0.80	−0.82/−0.82	−0.70/−0.70	−0.64/−0.64
O_d[b]	−0.65/−0.65	−0.73/−0.73	−0.52/−0.52	−0.75/−0.75	−0.66/−0.66	−0.74/−0.74

[a] 1S, 1O, and 1N correspond to structures of Figure 3, while 1S−Co, 1O−Co, and 1N−Co are the same structures without Co. [b] O_v is the oxygen atom close to Co, and O_d is the other one.

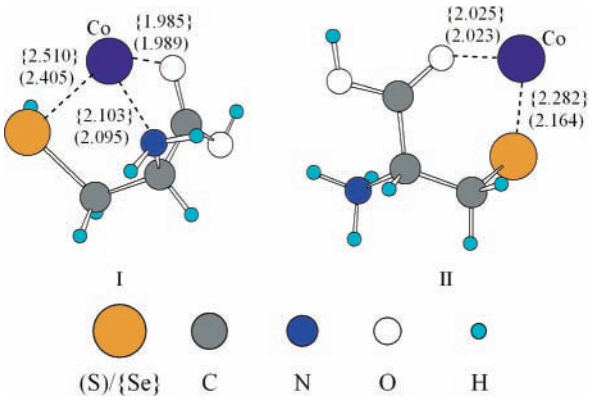

Figure 4. Structures of $[CoCys]^{2+}$ and $[CoSeCys]^{2+}$ complexes obtained from B3LYP/basisI geometry optimization. Some selected distances (in Å) are shown. Thick dashed lines correspond to bond critical points as suggested by AIM analysis.

we can remark that Co−S(Se) stretching modes are blue shifted in 1S structures with respect to those in 1O and 1N structures. Unfortunately, the intensities of these modes are very small, and the frequencies belong to a dense region of the IR spectrum, such that the different structures could not be experimentally determined by examining this region of the spectrum. δ_H is present in all structures. In 1S and 1N structures the δ_H peak is found at ∼1200 cm^{-1}, while in the 1O structure it is placed at 1099 cm^{-1}. In this last structure (1O) there is no H on oxygen, thus causing the difference in the δ_H peak location. $\nu_{C=O}$ has the most intense peak. This peak in the 1O structure is at 1828 cm^{-1}, while in 1S and 1N it is red shifted by about 100 cm^{-1}, being respectively at 1714 and 1698 cm^{-1}. Finally, the O−H stretching peak is evidently absent in the 1O structure, and it is at the same position for 1S and 1N structures (3700 cm^{-1}). In this region another peak (at 3590 cm^{-1}) in the 1N structure is relatively intense, while the corresponding peak in the 1S structure is at 3556 cm^{-1} with an intensity more than two times smaller (see the Supporting Information). Hence, an IR experiment in the gas phase could easily detect, eventually, the presence of a 1O structure (by the absence of ν_{OH} peak), while it is much more difficult to discriminate between 1S and 1N structures. Frequencies reported in this work are those directly obtained from DFT calculations without any rescaling. Note that it is well-known that the use of B3LYP functional needs a scale factor (usually ranging from 0.96 to 0.98 depending on the basis set and the frequency region[57,58]) to correctly reproduce experimental IR frequencies. These rescaling factors must be considered to directly compare our calculations with experiments when they will be available.

Finally, Co^{2+} complexes with neutral Cys and SeCys were also obtained at the B3LYP/basisI level. We investigated the two most stable structures, shown in Figure 4, taken from the two most stable $[Zn(II)Cys]^{2+}$ and $[Cd(II)Cys]^{2+}$ structures obtained by Belcastro et al.[50] In agreement with these calculations we found structure I more stable than structure II by 2.64 and 2.83 kcal/mol for Cys and SeCys, respectively. This result is in agreement with Zn^{2+} and Cd^{2+} results where the same order was found. Note that from ESI-MS experiments done in our laboratory by Buchmann and co-workers,[31] the $[CoCys]^{2+}$ species was not detected, and only the $[Co(Cys-H)]^+$ ion was obtained as the Co^{2+} monocysteine complex. Thus, we took into account only $[CoCys]^{2+}$ (and $[CoSeCys]^{2+}$) structures being the least in energy to determine the thermochemical analysis reported in what follows.

TABLE 6: Frequencies (in cm^{-1}) with Infrared Intensities in Parentheses (in km/mol) for Three $[Co(Cys-H)]^+$ and $[Co(SeCys-H)]^+$ Structures, Corresponding to the Following Modes: $\nu_{Co-S(Se)}$ Is the Co−S and Co−Se Stretching Mode, δ_H Is the Hydrogen Bending, $\nu_{C=O}$ Is the Carbonyl Stretching, and ν_{OH} Is the Stretching of OH Functions

$[Co(Cys-H)]^+$	$\nu_{Co-S(Se)}$	δ_H	$\nu_{C=O}$	ν_{OH}
1S	417(5.7)	1207 (123.2)	1714 (308.2)	3704 (201.9)
1O	246 (0.1)	1099 (166.4)	1828 (357.9)	-
1N	193 (2.7)	1180 (112.1)	1698 (275.0)	3703 (163.0)
		1201 (105.5)		
$[Co(SeCys-H)]^+$	$\nu_{Co-S(Se)}$	δ_H	$\nu_{C=O}$	ν_{OH}
1S	286 (7.7)	1205 (151.9)	1716 (303.0)	3705 (202.3)
1O	198 (5.4)	1100 (162.5)	1825 (362.4)	-
1N	170 (4.4)	1200 (126.5)	1700 (270.0)	3703 (162.2)

TABLE 7: Gas-Phase Metal Affinities (in kcal/mol) of Cys, [Cys-H] (Deprotonated Cysteine), SeCys, and [SeCys-H]

	Co^{2+}	Zn^{2+}	Cd^{2+}
Cys	237.66	214.5[a]	177.5[a]
Cys-H	461.16		
SeCys	242.55		
SeCys-H	460.54		

[a] Values taken from ref 50.

4.2. Thermochemical Analysis. Co^{2+} affinities for neutral and deprotonated Cys (SeCys) are shown in Table 7. In the same table we report also results obtained by Belcastro et al.[50] for Zn^{2+} and Cd^{2+} binding neutral cysteine. Cysteine metal affinity (MA) for Co^{2+} was found ∼23 kcal/mol greater than that for Zn^{2+} and ∼60 kcal/mol greater than that for Cd^{2+}. Co^{2+} MA with SeCys was found slightly higher than that with Cys (∼5 kcal/mol).

The MAs with deprotonated Cys and SeCys are ∼220 kcal/mol larger than those with neutral cysteine and selenocysteine. This effect is due to the tight binding between Co^{2+} and thiolate (and selenolate) functions that presents a high degree of covalent bonding, as pointed out in section 4.1. This higher affinity for deprotonated cysteine is in agreement with ESI-MS experiments results, finding the $[Co(Cys-H)]^+$ species in the spectra but not $[CoCys]^{2+}$. Hence, these experiments can be explained by the fact that Co^{2+} binds a deprotonated Cys, and an almost covalent bond is formed between the metal and the thiolate function. Our DFT study suggests that a similar behavior is expected for Se. On the other hand, if Co^{2+} binds a neutral Cys (SeCys) with a protonated thiol (seleniol) function the interaction

between cobalt and sulfur (selenium) is mainly electrostatic, without any relevant charge transfer between the metal and S (Se).

Finally, a large effect of Co^{2+} complexation on Cys (SeCys) reactivity was pointed out for the deprotonation reaction of such a complex. In Table 3 we also show ΔH^0_{298} and ΔG^0_{298} of the Cys (SeCys) deprotonation reaction when a Co^{2+} cation is binding. Comparing these values with the same obtained for free Cys (SeCys), we can immediately note that the energy needed for deprotonating a Co(II)−cysteine (selenocysteine) complex in the gas phase is about three times smaller than those needed for free Cys (SeCys). In both cases the deprotonated function is the thiol (seleniol) group. This means that the acidity of the thiol (seleniol) group is enhanced significantly by Co(II) binding. This can indirectly explain the formation of the S−Co binding motif in solution or in biological systems where a SH group at neutral or physiological pH is even expected to be protonated from its free-cysteine known pK_a of 8.

5. Conclusions

In this paper we have studied theoretically Co^{2+} binding to cysteine and selenocysteine using the DFT approach within the B3LYP functional. Here, we detailed energies, geometries, charge distributions, and vibrational analysis of different conformers that could be detected during gas-phase experiments, providing useful results for a better rationalization of these experiments. Analyzing the conformers of the amino acids in both neutral and deprotonated forms without and in the presence of the binding Co(II) metal, we are able to illustrate some aspects of the reactivity of these systems. In particular, the deprotonation reaction of SH and SeH acid functions in the bound cysteine and selenocysteine complexes is enhanced in the gas phase with respect to the cobalt free amino acids in the same gas phase. Different results of our investigation agree with this picture: (i) the SH (SeH) function is the most favorable deprotonation site among the possible ones; (ii) natural population analysis partially explains this phenomenon through a partial (and unique) charge transfer between S (Se) and cobalt (similar conclusions are also obtained by a more detailed investigation of chemical bond properties using NBO and AIM analysis); and (iii) thermochemical analysis provides a clear preferential affinity of Co(II) with deprotonated cysteine rather than with neutral one. This is confirmed by a drop in enthalpy and free energy differences for gas-phase deprotonation reactions in $[CoCys]^{2+}$ (and $[CoSeCys]^{2+}$) with respect to Cys (and SeCys) of a factor of three.

These results suggest a metal-assisted deprotonation reaction, as observed in cysteine complexes with other transition-metal cations[17,59,60] explaining the fragments produced during ESI-MS experiments done on cysteine−Co(II) complexes by our group.[31] (More details on the interactions in cysteine−Co(II) complexes characterized by ESI-MS/MS experiments will be given elsewhere.[33])

The substitution of S by Se does not change drastically the intrinsic reactivity of the amino acid with Co^{2+}. On one hand, this result provides further justification of selenium substitution in X-ray absorption spectroscopy on metalloproteins. On the other hand, it cannot explain the different biological behaviors of selenoproteins in metal detoxification. An evident possibility is that the biological specificity of Se is due to a different reactivity with respect to other reactions involved in the overall metal chelation process. Notably, a S−S bridge is present in a crucial step of metal binding in metallothioneines.[22] Thus the different reactivity of S−S, S−Se, and Se−Se bridges, as recently pointed out theoretically by Bachrach et al.,[61] can be at the origin of selenium biospecificity. Our current investigation, both theoretically and experimentally, is actually going in this direction.

Acknowledgment. This work was supported by the French Nuclear and Environmental Toxicology program. The authors thank W. Buchmann, M.-P. Gaigeot, and P. Vitorge for very fruitful discussions.

Supporting Information Available: Frequencies and infrared intensities for three $[Co(Cys-H)]^+$ and $[Co(SeCys-H)]^+$ structures. This material is available free of charge via the Internet at http://pubs.acs.org.

References and Notes

(1) Rodgers, M. T.; Armentrout, P. B. *Acc. Chem. Res.* **2004**, *37*, 989−998.
(2) Hu, P.; Loo, J. A. *J. Am. Chem. Soc.* **1995**, *117*, 11314−11319.
(3) Hoyau, S.; Ohanessian, G. *J. Am. Chem. Soc.* **1997**, *119*, 2016−2024.
(4) Rogalewicz, F.; Hoppilliard, Y.; Ohanessian, G. *Int. J. Mass Spectrom.* **2000**, *201*, 307−320.
(5) Strittmatter, E. F.; Lemoff, A. S.; Williams, E. R. *J. Phys. Chem. A* **2000**, *104*, 9793.
(6) Lemoff, A. S.; Bush, M. F.; Wu, C. C.; Williams, E. R. *J. Am. Chem. Soc.* **2005**, *127*, 10276−10286.
(7) Sigel, H.; Martin, R. B. *Chem. Rev.* **1982**, *82*, 385−426.
(8) Wang, J. P.; El-Sayed, M. A. *Photochem. Photobiol.* **2001**, *73*, 564−571.
(9) Joyce, G. F. *Annu. Rev. Biochem.* **2004**, *73*, 791−836.
(10) El-Sayed, M. A.; Yang, D. F.; Yoo, S. K.; Zhang, N. *Isr. J. Chem.* **1995**, *35*, 465−474.
(11) Arnold, A. P.; Stanley, D. M.; Collins, J. G. *FEBS Lett.* **1995**, *289*, 96−98.
(12) Gooding, J. J.; Hibbert, D. B.; Yang, W. *Sensors* **2001**, *1*, 75−90.
(13) Mathe, C.; Mattioli, T. A.; Horner, O.; Lombard, M.; Latour, J. M.; Fontecave, M.; Niviere, V. *J. Am. Chem. Soc.* **2002**, *124*, 4966−4967.
(14) Miyanaga, A.; Fushinobu, S.; Ito, K.; Wakagi, T. *Biochem. Biophys. Res. Commun.* **2001**, *288*, 1169−1174.
(15) Endo, I.; Nojiri, M.; Tsujimura, M.; Nakasako, M.; Yohda, M.; Odaka, M. *J. Inorg. Biochem.* **2001**, *83*, 247−253.
(16) Meinnel, T.; Blanquet, S.; Dardel, F. *J. Mol. Biol.* **1996**, *262*, 375−386.
(17) Simonson, T.; Calimet, N. *Proteins: Struct., Funct., Genet.* **2002**, *49*, 37−48.
(18) Dawson, R. M. C.; Elliot, D. C.; Elliot, W. H.; Jones, K. M. *Data for Biochemical Resarch*, 3rd ed.; Clarendon Press: Oxford: 1995.
(19) *Handbook of Chemistry and Physics*; Lide, D. R., Ed.; CRC Press: Boca Raton, FL, 1998.
(20) Bombarda, E.; Morellet, N.; Cherradi, H.; Spiess, B.; Bouaziz, S.; Grell, E.; Roques, B. P.; Mely, Y. *J. Mol. Biol.* **2001**, *310*, 659−672.
(21) Hightower, K. E.; C.-C. Huang,; Casey, P. J.; Fierke, C. A. *Biochemistry* **1998**, *37*, 15555−15562.
(22) Jacob, C.; Giles, G. I.; Giles, N. M.; Sies, H. *Angew. Chem., Int. Ed.* **2003**, *42*, 4742−4758.
(23) Chen, J.; Berry, M. J. *J. Neurochem.* **2003**, *86*, 1−12.
(24) Behne, D.; Kyriakopoulos, A. *Annu. Rev. Nutr.* **2001**, *21*, 453−473.
(25) Schomburg, L.; Schweizer, U.; Holtmann, B.; Flohe, L.; Sendtner, M.; Köhrle, J. *Biochem. J.* **2003**, *370*, 397−402.
(26) Hill, K. E.; Zhou, J.; McMahan, W. J.; Motley, A. K.; Atkins, J. F.; Gesteland, R. F.; Burk, R. F. *J. Biol. Chem.* **2003**, *278*, 13640−13646.
(27) Goyer, R. A. *Annu. Rev. Nutr.* **1997**, *17*, 37−50.
(28) Othman, A. I.; El Missiry, M. A. *J. Biochem. Mol. Toxicol.* **1998**, *12*, 345−349.
(29) Peariso, K.; Zhou, Z. Z.; Smith, A. E.; Matthews, R. W.; Penner-Hahn, J. E. *Biochemistry* **2001**, *40*, 987−993.
(30) Ralle, M.; Berry, S. M.; Nilges, M. J.; Gieselman, M. D.; van der Donk, W. A.; Lu, Y.; Blackburn, N. J. *J. Am. Chem. Soc.* **2005**, *126*, 7244−7256.
(31) Tournois, G.; Buchmann, W.; Tortajada, J.; Cartailler, T. *Proceedings of the 53rd ASMS Conference, San Antonio (TX)*, 2005; MP 318.
(32) Spezia, R.; Tournois, G.; Tortajada, J.; Cartailler, T.; Gaigeot, M.-P. *Phys. Chem. Chem. Phys.* **2006**, *8*, 2040−2050.
(33) Tournois, G.; Buchmann, W.; Spezia, R.; Cartailler, T.; Tortajada, J. **2006**, manuscript in preparation.
(34) Becke, A. D. *J. Chem. Phys.* **1993**, *98*, 5648−5652.

(35) Holthausen, M. C.; Mohr, M.; Koch, W. *Chem. Phys. Lett.* **1995**, *240*, 245−252.
(36) Blomberg, M. R. A.; Siegbahn, P. E. M.; Svensson, M. *J. Chem. Phys.* **1996**, *104*, 9546−9554.
(37) Liu, C.; Zhang, D.; Bian, W. *J. Phys. Chem. A* **2003**, *107*, 8618−8622.
(38) Constantino, E.; Rodriguez-Santiago, L.; Sodupe, M.; Tortajada, J. *J. Phys. Chem. A* **2005**, *109*, 224−230.
(39) Constantino, E.; Rimola, A.; Rodriguez-Santiago, L.; Sodupe, M. *New J. Chem.* **2005**, *29*, 1585−1593.
(40) Wachters, A. J. H. *J. Chem. Phys.* **1970**, *52*, 1033−1036.
(41) Hay, P. J. *J. Chem. Phys.* **1977**, *66*, 4377−4384.
(42) Raghavachari, K.; Trucks, G. W. *J. Chem. Phys.* **1989**, *91*, 1062−1065.
(43) Weinhold, F.; Carpenter, J. E. *The Structure of Small Molecules and Ions*; Plenum: New York: 1988.
(44) Carpenter, J. E.; Weinhold, F. *J. Mol. Struct. (THEOCHEM)* **1988**, *169*, 41−62.
(45) Cotton, F. A.; Wilkinson, G. *Advanced Inorganic Chemistry;* John Wiley and Sons: New York, 1980.
(46) Chillemi, G.; D'Angelo, P.; Pavel, N. V.; Sanna, N.; Barone, V. *J. Am. Chem. Soc.* **2002**, *124*, 1968−1976.
(47) Frisch, J. R. et al. *Gaussian 98*; Gaussian Inc.: Pittsburgh, PA, 1998.
(48) McQuarrie, D. A. *Statistical Thermodynamics*; Harper and Row: New York, 1973.
(49) Boys, S. F.; Bernardi, F. *Mol. Phys.* **1970**, *19*, 553−566.
(50) Belcastro, M.; Marino, T.; Russo, N.; Toscano, M. *J. Mass. Spectrom.* **2005**, *40*, 300−306.
(51) Hoyau, S.; Norrman, K.; McMahon, T. B.; Ohanessian, G. *J. Am. Chem. Soc.* **1999**, *121*, 8864−8875.
(52) Noguera, M.; Rodriguez-Santiago, L.; Sodupe, M.; Bertran, J. *J. Mol. Struct. (THEOCHEM)* **2001**, *537*, 307−318.
(53) Hunter, E. P.; Lias, S. G. *J. Phys. Chem. Ref. Data* **1998**, *27*, 413−656.
(54) O'Hair, R. A. J.; Bowie, J. H.; Gronert, S. *Int. J. Mass Spectrom. Ion Proc.* **1992**, *117*, 23−36.
(55) Bader, R. F. W. *Atoms in Molecules: A Quantum Theory;* Oxford University Press: Oxford: 1990.
(56) Cioslowski, J.; Nanayakkara, A.; Challacombe, M. *Chem. Phys. Lett.* **1993**, *203*, 137−142.
(57) Foresman, J. B.; Frish, E. *Exploring Chemistry with Electronic Structure Methods*, 2nd ed.; Gaussian Inc.: Pittsburgh, PA, 1996.
(58) Halls, M. D.; Velkovski, J.; Schlegel, H. B. *Theor. Chem. Acc.* **2001**, *105*, 413−421.
(59) Dudev, T.; Lim, C. *J. Am. Chem. Soc.* **2002**, *124*, 6759−6766.
(60) Burford, N.; Eelman, M.; Groom, K. *J. Inorg. Biochem.* **2005**, *99*, 1992−1997.
(61) Bachrach, S. M.; Demoin, D. W.; Luk, M.; Miller, J. V., Jr. *J. Phys. Chem. A* **2004**, *108*, 4040−4046.